

Intrusion and differentiation of granitic magma at a high level in the crust: the Puscao pluton, Lima Province, Peru

by W. P. TAYLOR

Department of Geology, University of Liverpool

(Received 31 July 1974; in revised form 11 June 1975)

ABSTRACT

Regression surface techniques have been used on partial whole-rock chemical analyses from the Puscao pluton to establish the three-dimensional nature of the chemical variations within this body, which was emplaced at a depth of between 4 km and 8 km within the crust. Block diagrams produced by the computer program are consistent with the hypothesis that during the period preceding the total consolidation of the magma, the pluton has undergone *in situ* differentiation to give a layered structure.

Statistical analysis confirms that there is a large scale variation within the pluton and that local variation, such as might be expected to result from the contamination of the Puscao magma by assimilated volcanic material, did not contribute significantly to the overall variation.

Evidence is presented which suggests that the layering within the Puscao pluton was disturbed as a result of the emplacement of the much later Cañas pluton, and that this disturbance has the form of a simple doming centred upon the site of the present Cañas intrusion.

INTRODUCTION

Geological setting

Successive workers in the whole of the 1300 km long Coastal Batholith of Peru, like their counterparts in North America, have evolved an increasingly complex picture of the emplacement of large volumes of magma at high levels within the crust. In the Coastal Batholith, as within the rest of the Circum-Pacific batholiths, the basic and acidic magmas appear to be temporally related, with more basic intrusions usually predating the later more acid members of the sequence.

Cobbing & Pitcher (1972) noted this gross basic-acid cycle which gave rise to the major bodies of gabbro, diorite, quartz diorite, tonalite, granodiorite, and adamellite.

The batholith is composed mainly of tonalites and earlier gabbros. Granodiorite and adamellite bodies are usually confined to rather localized centres of intrusive activity which occur at intervals along the median line of the batholith. These late multiple intrusive complexes, although having a common or very restricted locus of intrusive activity, may or may not have ring dykes associated with them. The term centred complex is therefore adopted in this paper in

preference to the more restrictive term ring complex, even though the presence of a ring dyke in the particular complex involved makes either term equally applicable.

The Puscao pluton is one of the units which make up the Huaura Centred Complex in Lima Province. This complex is cut by the Rio Huaura in the area around Sayán and sharp contacts between the several units and the roof may be observed on either flank of the river and in the many dry valleys or quebradas. A generalized map of the Huaura Centred Complex shown in Fig. 1 contains most of the important features of the complex.

Cobbing & Pitcher (*op. cit.*) have shown that the focus of intrusive activity does not appear to have remained stationary during the period of emplacement of the complex. After the initial phase of intrusion in the southern part of the complex, the focus of activity migrated northwards so that the later intrusions now occur as a less obviously centred group mainly to the north of the river. The northern centre has as its oldest member the Puscao unit and the arrival into place of the steep-sided, circular Cañas stock was the final event in the intrusive history of the complex.

Cobbing & Pitcher (*op. cit.*) show that the emplacement of the complex involved cauldron subsidence along arcuate fractures associated with ring dykes and cone sheets, and the engulfment of huge blocks. Such a mode of emplacement is consistent with their belief that the intrusive process took place at a high level in the crust and this assumption is in accord with the findings of Atherton & Brenchley (1972) who show, from their study of the contact metamorphism of the aureole some 70 km to the northwest of Sayán, that the batholith was emplaced under pressure and temperature conditions of 1–2 kb and 530–600 °C.

In the case of the Huaura Complex, therefore, one is dealing with a centred complex which was emplaced in the epizone (Buddington, 1959) and was very likely to have had sub-volcanic associations similar to those of the Rio Fortaleza Centre further to the north, described by Knox (1974).

The author has been particularly interested in the Puscao unit which is now discussed in some detail.

The Puscao unit

The Puscao unit, part of which is shown in Fig. 1, trends NW.–SE. and is 65 km long and up to 20 km wide.

This rather simplified picture of the intrusion is however complicated by certain features which are as follows:

(a) In the southern part of the intrusion major extensions of a later adamellite cut across the Puscao unit causing a fragmentation of the outcrop pattern.

(b) 3 km to the north of the Quebrada Tumaray a body of meladiorite representing pendant roof material breaks the apparent continuity of the body,

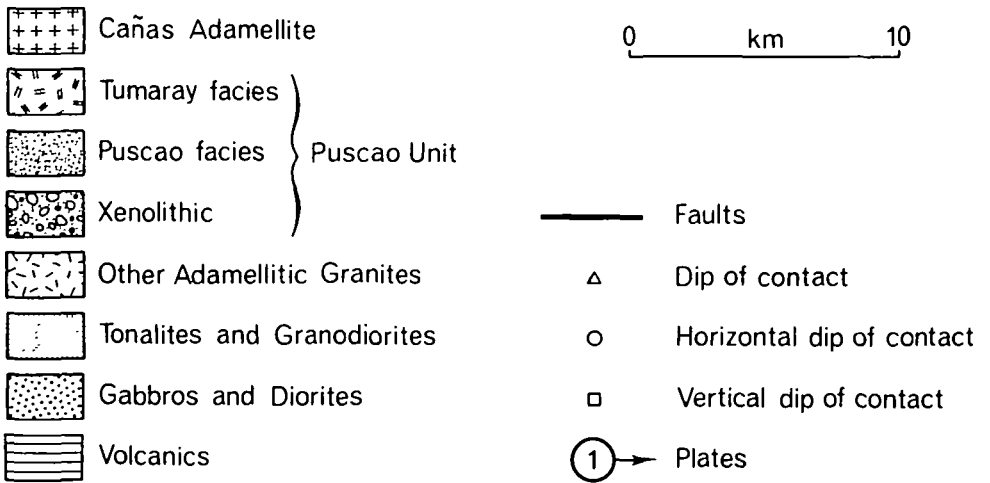
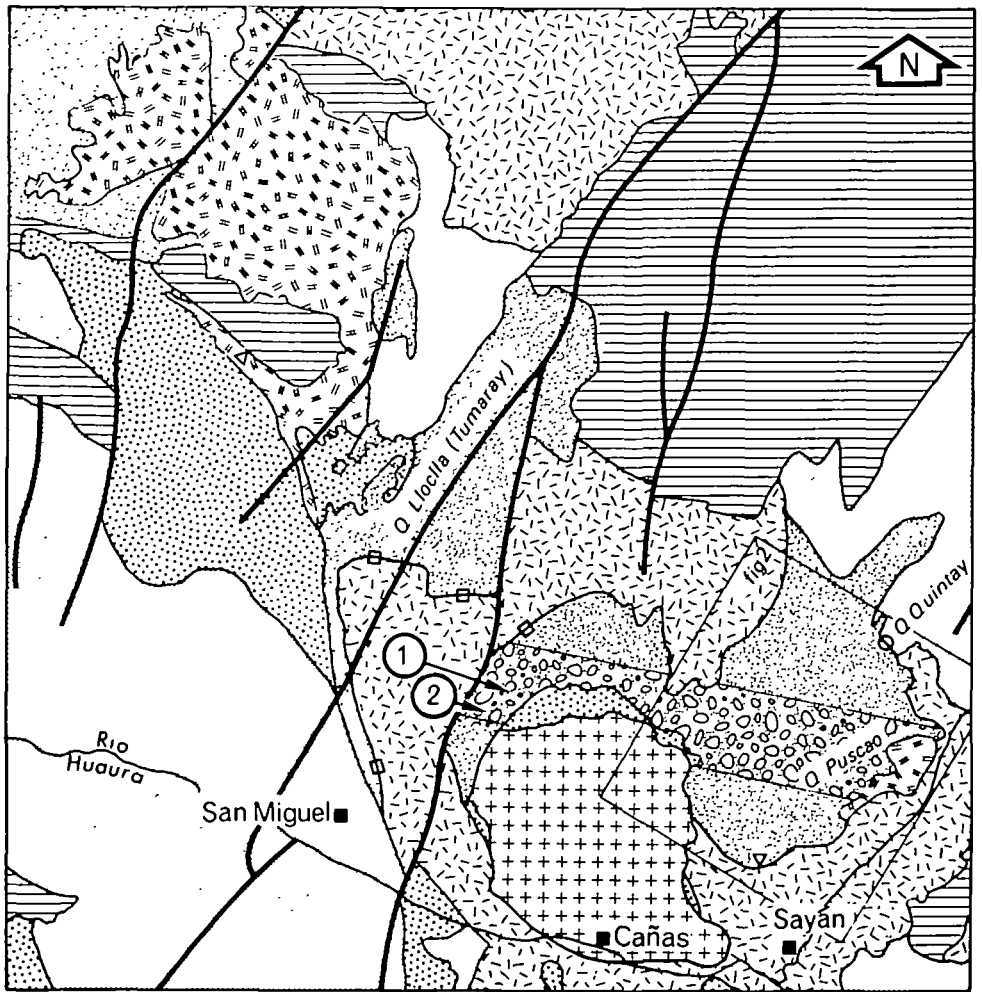


FIG. 1. Generalized map of the Huaura Complex showing the relationship of the Puscao pluton to its surroundings (after Cobbing & Pitcher, 1972).

but the presence of apophyses of adamellite within the meladiorite leave the author in little doubt that the Puscao intrusion is continuous at no great depth.

The attitude of the contact with the country rock is somewhat variable; horizontal against the earlier tonalite in Quebrada Quintay and the eastern volcanics further to the north, or steeply dipping outwards at its northern extremity. These contact relationships and the presence of the roof pendant material suggests that one is dealing with the uppermost part of a flat-roofed, steep sided pluton.

The Puscao unit covers such an areal extent that it intrudes a wide spectrum of country rock, from the envelope volcanics, early diorites, meladiorites, and gabbros, to the more acid members such as the tonalites and granodiorites.

Petrologically, the Puscao unit exhibits pronounced facies variations which are easily recognizable in the field. There are three main facies within the unit and these are usually referred to as the Adamellitic Puscao facies, the Tumaray Aplitic facies and a 'Basified' Xenolithic facies. Such facies variants within the Puscao unit tend to be arranged in such a manner as to give rise to an overall large scale layered structure, and Cobbing & Pitcher (*op. cit.*) describe mountains in the northern part of the pluton which consist in the main of adamellite, have aplitic tops, and at the foot (some 700 m below) are composed of the xenolithic variant.

Within the basified facies the xenoliths themselves appear to reflect this large scale layering since they are concentrated in xenolith-rich horizons which dip at very low angles towards the south.

Cobbing & Pitcher (*op. cit.*) mention two thick shallowly dipping bands of the basified facies in the Huaura area, in which plate-like xenoliths (5–20 cm long) lie parallel to the overall dip of the bands. These authors, like the present author, consider that the xenoliths, which are now aggregates of fine acicular hornblende, biotite, and feldspar, are remnants of disrupted, spalled-off flakes of the roof volcanics. The general field appearance of these xenoliths is shown in Plate 1A.

One of these bands of xenolith-charged basified facies occurs in the area to the north of Sayán which is shown on the map in Fig. 1, and which was investigated in detail by the present author. Here the adamellite of the Puscao Adamellitic facies with its well dispersed flakes of biotite and well formed prisms of hornblende grades, as a result of increased amounts of hornblende, into the basified facies.

Indeed Cobbing & Pitcher (*op. cit.*) believed that the mentioned 'basification' of the adamellite was due to the assimilation of xenolithic material, since there appeared to be an exact correlation between the xenolith density and the colour index of the host, with xenoliths being found in varying stages of assimilation.

On the basis of this evidence, the Puscao pluton was chosen for an investigation of the effects of contamination on magma *after* its emplacement.

GEOCHEMISTRY OF THE PUSCAO PLUTON

In view of the many square kilometres of terrain which Cobbing & Pitcher (*op. cit.*) envisage as being affected by xenolithic contamination, and because of the strong relief resulting from the comparatively recent uplift of the Andean chain, the present author decided that the techniques of regression surface analysis would be ideally suited to this type of study.

Sampling of the pluton

The outline of the Puscao pluton was drawn on aerial photograph No. 1509 (Instituto Geographico Militar del Peru), together with lines separating that part of the pluton in which there are numerous xenoliths from that part of the pluton in which the xenoliths are virtually absent. This revealed an interesting fact that the xenoliths appear to be confined to a parallel-sided belt of the pluton some 5 km in width and trending WNW.–ESE. whose straight line margins on the photograph must represent vertical planes in such strongly dissected terrain.

Since it was thought that the contamination of the pluton was directly associated with this belt of xenoliths, the dimensions of the 5×5 square sampling grid were chosen such that when half of the localities lay within this belt the square grid would occupy as much of the pluton as possible (Fig. 2).

The author visited each of the grid localities marked on the aerial photograph and measured their heights using a pocket altimeter. Several of the heights obtained in this way were remeasured and the results never varied by more than three metres from their original values.

Eight samples were collected at each locality by taking one sample at a distance of 20 m from the centre of the locality, towards each of the major compass points. Fresh, unweathered samples were taken using a sledge-hammer, with considerable care being exercised to ensure that the fragments consisted entirely of the host rock, and any schlieren, xenolithic material, basic dykes or aplitic veins were not included in the sample. The size of specimen collected enabled 400 g to be crushed for analysis and still leave a large enough portion to enable thin sections to be produced from any of the specimens.

The sample weight was estimated using the results of Southern Californian workers, *e.g.* Baird *et al.* (1967), and on returning to the laboratory, analysis of the two halves of an 800 g sample confirmed the adequacy of the sample size.

Geochemical analysis and initial treatment of the data

The 200 (*i.e.* 25×8) samples were individually analysed by automated wet chemical methods for the oxides of sodium, potassium, calcium, magnesium, total iron, and titanium.

The methods themselves are discussed by Atherton *et al.* (1971) and Table 1 shows their values for the percentage relative deviations, and those achieved by

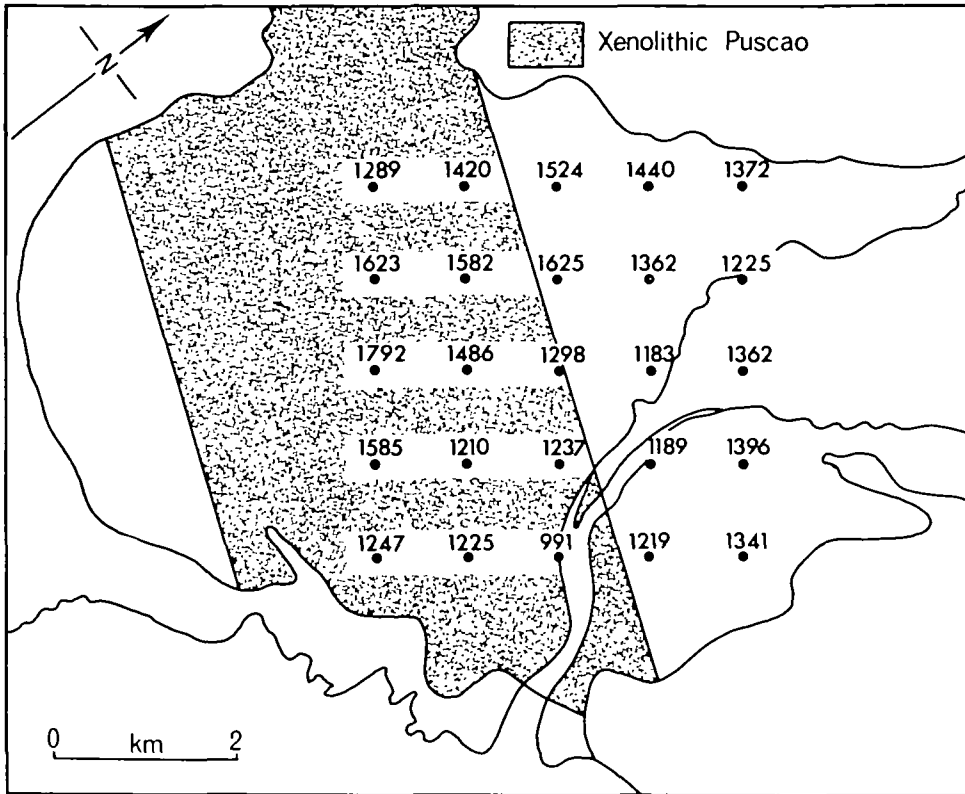


FIG. 2. Sampling plan for the Puscao pluton with locality elevations shown in metres.

the present author as a result of analysing the same Puscao specimen on thirteen separate occasions as a 'quality-control' during the analytical scheme. Since precisely the same instrumental configuration was used, the similarity between the values is hardly surprising and the present author's higher percentage relative

TABLE 1

Comparison of the analytical variance for the Puscao Pluton with that achieved by previous workers elsewhere

Oxide	δ (Analytical variance)	Mean value	Percentage relative deviation		
			Mercy (1956)	Atherton et al. (1971)	Present author
TiO ₂	3.73×10^{-3}	0.3586	6.9	0.79	1.04
Fe ₂ O ₃	7.18×10^{-2}	3.375	2.1	0.56	2.13
MgO	1.92×10^{-2}	1.160	2.2	0.78	1.66
CaO	3.10×10^{-2}	3.329	0.88	0.97	0.93
Na ₂ O	2.21×10^{-2}	4.138	1.8	0.85	0.53
K ₂ O	3.48×10^{-2}	2.525	3.0	0.86	1.38

deviation for total iron may be a reflection of the fact that his rocks contain less than half the total iron present in the sample used by Atherton *et al.* (*op. cit.*).

Before any study of the large scale variation within the pluton could be embarked upon, it was necessary to confirm that the variance at this large scale was significantly greater than could be reasonably explained in terms of the small scale and analytical variances.

An estimate of the within-locality variance could have been computed without the need for eight individual analyses at all of the localities, but extra information could, if necessary, be used in a detailed comparison of the variation inside and outside the xenolithic belt.

Snedecor's F test was used to compare the analytical variance and the within-locality variance for each oxide, and showed that the within-locality variance is significantly greater than the analytical variation (exceeding the 99.95 per cent level).

The F test was also used to compare the within-locality and between-locality variance for each oxide, and showed that the between-locality variance is significantly greater than the within-locality variance. The lowest and highest values of F obtained at this stage in the analysis are shown in Table 2.

TABLE 2
Analysis of variance applied to the oxides of sodium and magnesium for the Puscao Pluton

Na ₂ O					
<i>Source of variation</i>	<i>S.S.</i>	<i>d.f.</i>	<i>Variance estimate</i>	<i>F</i>	<i>Percentage significance</i>
Between locality	2.4676	24	0.1028		
Within locality	1.3772	175	0.0079	13.1	99.9+
TOTAL	3.8448	199			
	<i>Grand mean = 3.84.</i>		<i>Analytical variance = 0.0005.</i>		
MgO					
<i>Source of variation</i>	<i>S.S.</i>	<i>d.f.</i>	<i>Variance estimate</i>	<i>F</i>	<i>Percentage significance</i>
Between locality	53.973	24	2.249		
Within locality	2.599	175	0.0149	151.4	99.9+
TOTAL	56.572	199			
	<i>Grand mean = 1.29.</i>		<i>Analytical variance = 0.0004.</i>		

S.S. signifies 'Sum of squares', and *d.f.* signifies 'Degrees of freedom'.

In order to gain more information about the large-scale variation which is present within the pluton, regression surface analysis techniques were then employed. The type of regression surfaces chosen represented a mathematical extension into three dimensions of the more familiar trend surfaces, thus enabl-

ing the effect of variation with height as well as variation with geographical location to be taken into account.

An indication of how well the sampling localities were distributed in three dimensions was obtained by calculating, for the sampling grid in Fig. 2, the ratio between the maximum elevation difference within each of the NW. and the NE. rows, to the length of the respective rows. The mean value for this ratio is 1:8 and its value never falls below 1:23.

The author considered the generation of regression surfaces up to, and including, the third degree (with its twenty coefficients) from only twenty-five data points to be justified on the following grounds:

(a) The highly significant large-scale variation, as illustrated in Table 2.

(b) The averaging of eight separate samples to obtain each locality value reduced the 'noise' contribution associated with that locality, and hence increased the probability that any flexures of the higher order surfaces represented actual large scale variations rather than very localized deviations.

(c) The good three dimensional distribution of the data as discussed above.

(d) Probably most important of all, the way in which the variation portrayed by these surfaces was consistent with the large-scale facies variations which had been observed in the field.

TABLE 3

The significance of added terms in the regression surface equations calculated by the method suggested by Chayes (1970)

Oxide	Order <i>n</i>	Ratio of the mean squares	Degrees of freedom		Percentage significance
			(a)	(b)	
K ₂ O	2	0.821	6	15	50+
	3	14.555	10	5	99.5
Na ₂ O	2	3.739	6	15	98.0
	3	4.062	10	5	93.0
TiO ₂	2	4.877	6	15	99.4
	3	2.815	10	5	85.0
CaO	2	3.975	6	15	98.0
	3	5.420	10	5	96.0
MgO	2	8.195	6	15	99.95
	3	5.548	10	5	96.0
Fe ₂ O ₃	2	6.813	6	15	99.8
	3	3.570	10	5	91.0

(a) are the degrees of freedom associated with terms of order *n*, and (b) are the degrees of freedom associated with the residual variation at order *n*.

A modified version of the program by Sampson and Davis (1967) was used to compute the regression surfaces for each oxide, in an attempt to show the three-dimensional variation within a 610 m thick, 4270 × 4270 m square block which encompasses most of the data points used in its computation.

To choose which order of regression surface to rely upon, Chayes (1970)

suggested that the mean square for variance associated with terms of order n should be tested against the mean square for the unexplained variation at order n , using Snedecor's Variance Ratio Test, to see if the terms of the n^{th} order improve the fit significantly or whether the fitting should rest at order $(n-1)$. The values of the ratio of the mean squares for the second and third order are presented for each oxide in Table 3, together with the appropriate degrees of freedom. In the light of the information from Table 3, the author decided to use the third order regression equations for all of the oxides, and the resulting block diagrams are shown in Figs. 3 and 4.

Each of the six block diagrams is characterized by a series of sub-horizontal layers, indicating the essentially vertical nature of the variation in percentage oxide. The amounts of the oxides of calcium, magnesium, titanium, sodium, and total iron show an increase in a downward sense, whereas for the oxide of potassium the reverse is true in that its amount shows an increase in the upward sense.

The values at the extremities of the block diagram may not represent realistic values since they lie at too great a distance from the data control points used in its construction. The central portion of the block diagram may, however, be used to provide realistic estimates of the amount of vertical variation in the percentage of each oxide.

Contamination or some other mechanism?

In Fig. 5 the average plots for each of the twenty-five sampling localities are shown on the selective enlargement of the central portion of the triangular diagram, which also contains the igneous differentiation trends discussed by Green & Poldervaart (1958).

The plotted values lie on a curve which almost coincides with the curve for calc-alkaline differentiation, as one might expect, and the plots themselves may be considered to fall into four fairly distinct groupings indicated by the use of different plotting symbols.

When the symbols from the triangular diagram are transferred to the sampling localities that they represent on the original sampling plan, a map such as that shown in Fig. 6 may be produced. There does not appear to be any relationship between the different groups of symbols and the xenolith belt, since curved lines may be drawn between the groups of symbols, and these lines are markedly oblique to the xenolith belt. This appears to be a very strong indication that contamination due to assimilation of basic material within the xenolith belt is not the main factor controlling oxide distributions in the pluton.

The distribution of the symbols in Fig. 6 does, however, appear to vary systematically towards the west.

If, as seems likely, the factor influencing the distribution of the symbols lies to the west then it almost certainly occurs outside the confines of the Puscao pluton, and must also post-date the emplacement of the latter.

Consideration of the geology to the west of the sampled area reveals that

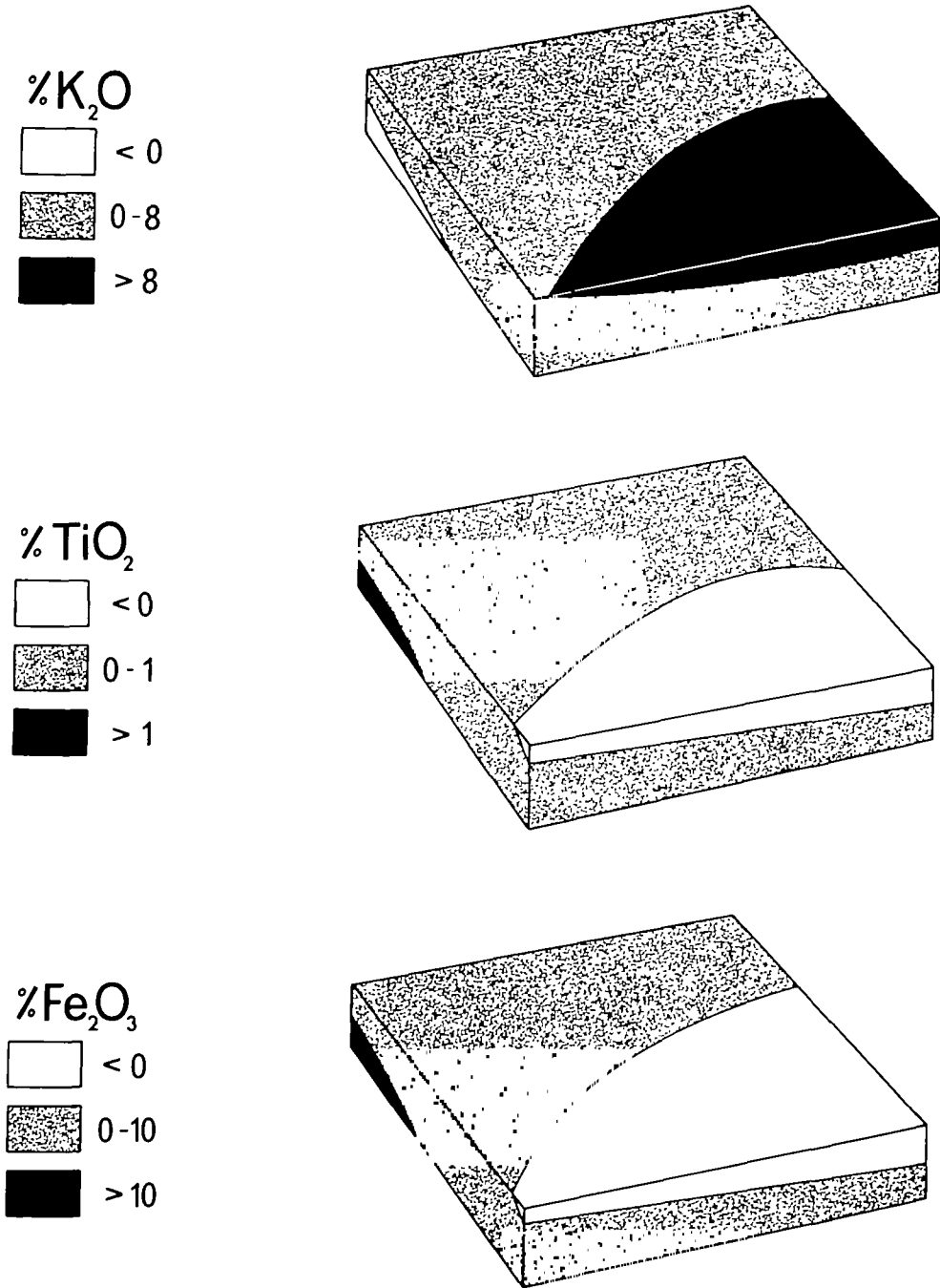


FIG. 3. Block diagrams showing the potassium, titanium, and total iron oxide distributions within the Puscao pluton. The dimensions of the block are 4270 × 4270 m with the upper face at 1680 m and the lower one at 1070 m.

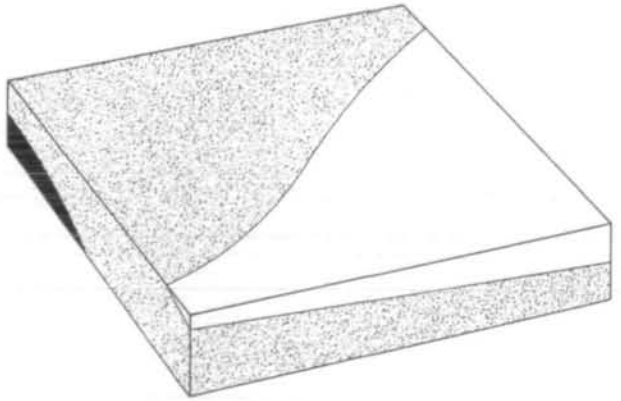
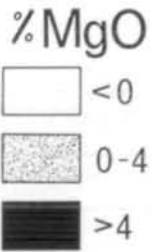
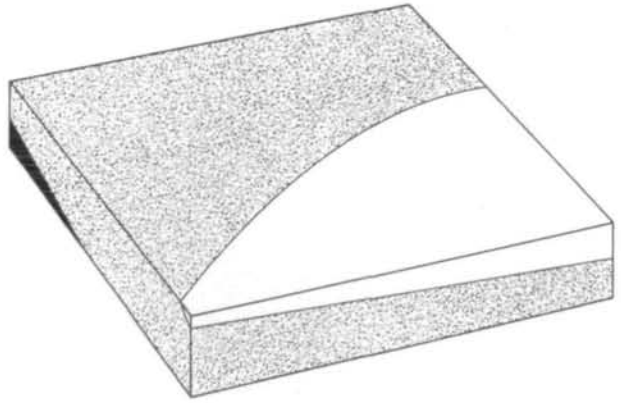
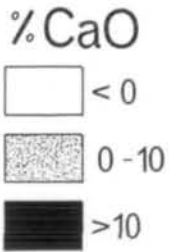
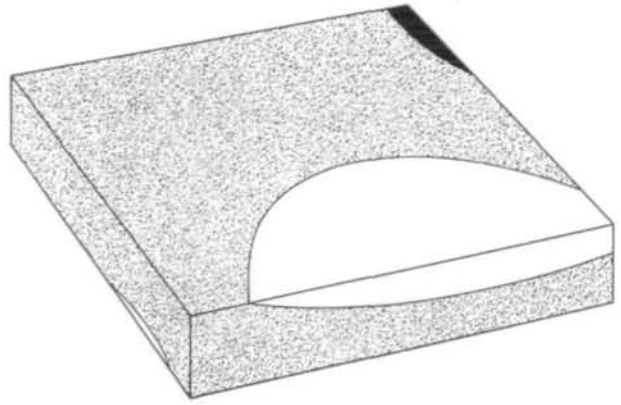
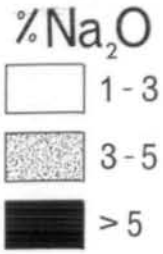


FIG. 4. Block diagrams showing the sodium, calcium, and magnesium oxide distributions within the Puscao pluton. The dimensions of the block are 4270×4270 m with the upper face at 1680 m and the lower one at 1070 m.

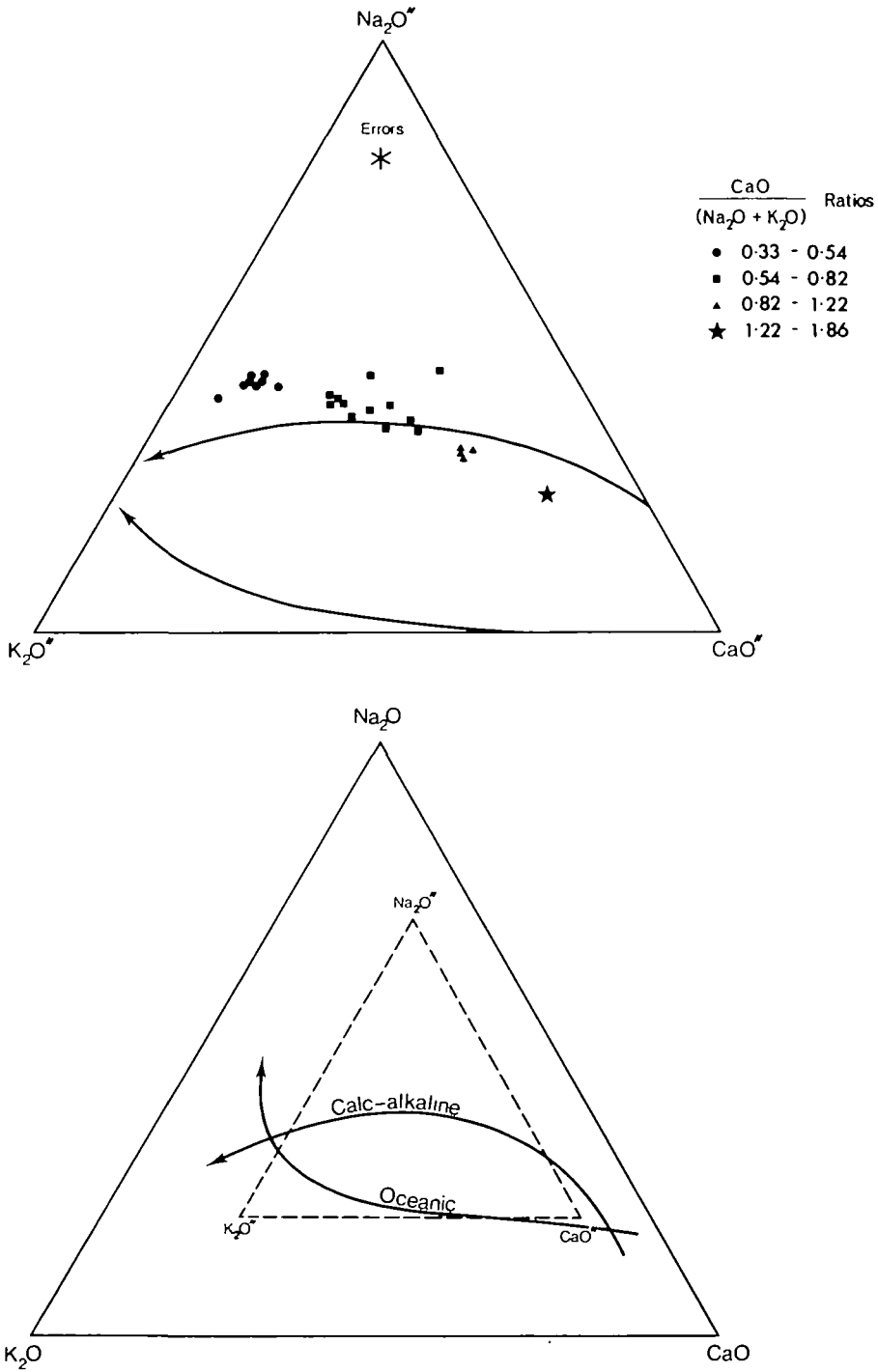


FIG. 5. Three component diagrams showing the distribution of the Puscao data (after Green & Poldervaart, 1958).

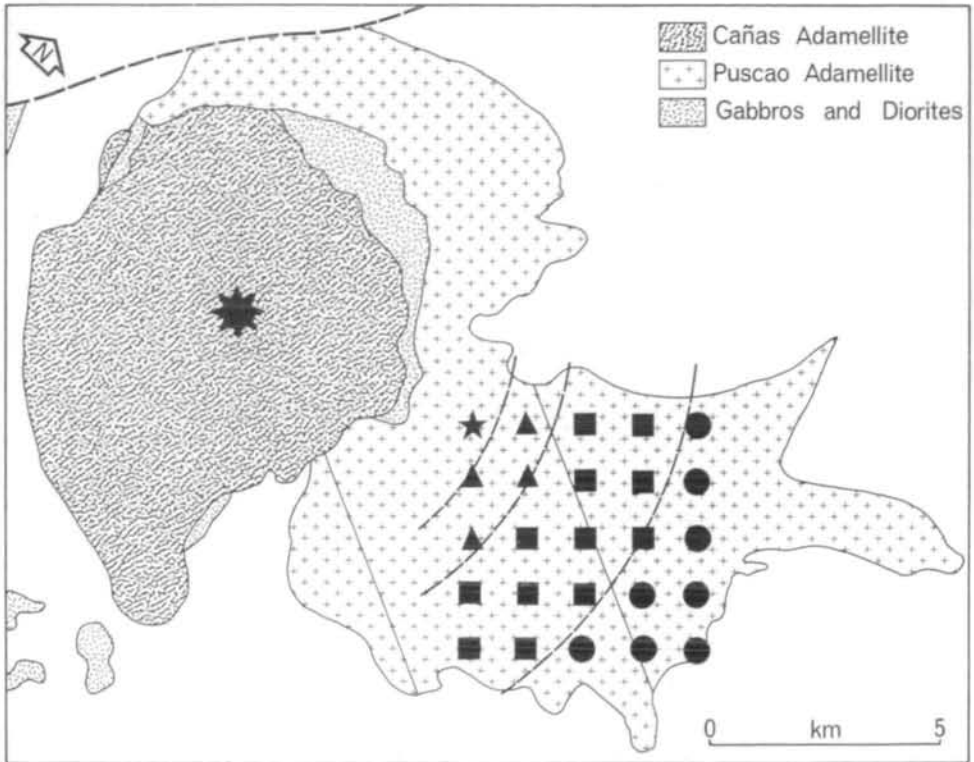


FIG. 6. Map showing how the oxide distributions within the Puscao pluton are related to the later Cañas pluton. Symbols represent the same ranges of $\text{CaO}/(\text{Na}_2\text{O} + \text{K}_2\text{O})$ as those in Fig. 5.

there is only one later intrusion which could possibly have produced the observed distribution, the Cañas pluton.

The Cañas pluton occupies such a compact area in relation to the adjacent Puscao pluton that when the observations are considered in terms of the possible effects of the Cañas pluton, the evidence is unfortunately confined to a rather limited sector. There does not, however, appear to be any reason for supposing that this sector is atypical in its relationship to the Cañas pluton, and the author feels that one might reasonably expect any effect due to the circular Cañas pluton to be radially disposed.

Acceptance of the radial nature of the influence of the Cañas pluton would also explain the apparent curvature of the lines separating the different symbols in Fig. 6, since these lines would then be the arcs of a series of concentric circles, having their common centre at or near the geometrical centre of the Cañas pluton (the star on Fig. 6).

In an attempt to clarify the relative merits of the original concept based on xenolithic contamination, and the new idea of a distribution which is radially related to the Cañas pluton, two types of graphs were plotted. In the first case the mean of eight analyses for each locality (plus or minus one standard devia-

tion) was plotted against the distance from the margin of the xenolith belt, such that measurements within the 'contaminated' part were plotted to the left of the vertical axis and those outside the belt were plotted to the right. In the second case the same locality means were plotted against the radial distance from the geometrical centre of the Cañas pluton.

The results obtained using the two methods of plotting described above are presented in Figs. 7 and 8. A marked increase in the linear correlation occurs when the radial type of plot is utilized, so marked in fact that it may be appreciated by a simple visual comparison of the corresponding pairs of graphs. The values of the linear correlation coefficient 'r' have been computed for the radially plotted graphs and are shown in Figs. 7 and 8.

The apparent radial nature of the oxide distribution around the Cañas pluton confirms what little part xenolithic contamination has played in the large-scale chemistry of the body, though the presence of reaction rims around some of the xenoliths suggests that contamination must have played a part at the very local scale. This localized contamination effect manifests itself as an increase in the within-locality variance. In the case of magnesium oxide, for example, Snedecor's F test may be used to demonstrate a very significant difference between the within-locality variances for localities lying within the xenolith belt and those for localities outside the belt, as may be seen in Table 4.

TABLE 4

Comparison of magnesium oxide within-locality variance for localities inside the xenolith belt with that for localities outside the belt

<i>Estimate of within-locality variance</i>		<i>Degrees of freedom</i>	<i>F</i>	<i>Percentage significance</i>
Inside the xenolith belt	0.02524	91	7.11	.99.9+
Outside the xenolith belt	0.00355	84		

It is possible to summarize the salient features of the radially plotted graphs (Figs. 7 and 8) as follows:

(a) The approximate position of the contact of the Cañas pluton is at 4 km on the radial scale.

(b) The amounts of the oxides of calcium, magnesium, titanium, and total iron increase towards the Cañas pluton.

(c) The amount of the oxide of potassium *decreases* towards the Cañas pluton.

(d) In the case of the oxide of sodium there is little variation in amount when considered both in the light of the analytical error as represented by the error bars, and the rather poor value for the linear correlation coefficient.

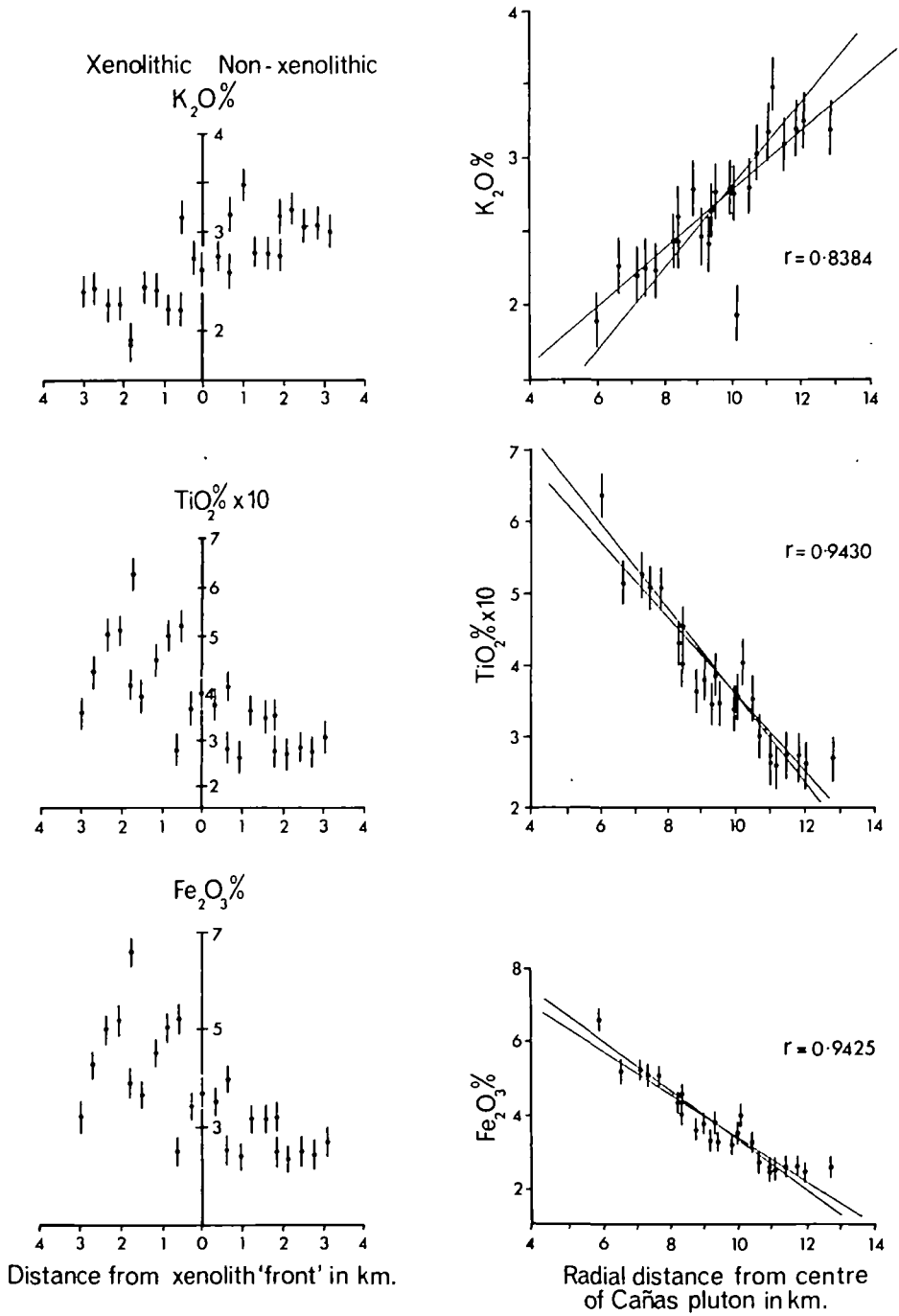


FIG. 7. Graphs showing the percentage of potassium, titanium, and total iron oxides as a function of the distance from the xenolith 'front', and as a function of the radial distance from the centre of the Cañas pluton. In the graphs on the left-hand side of the figure, values from within the xenolith belt are plotted to the left of the central axis.

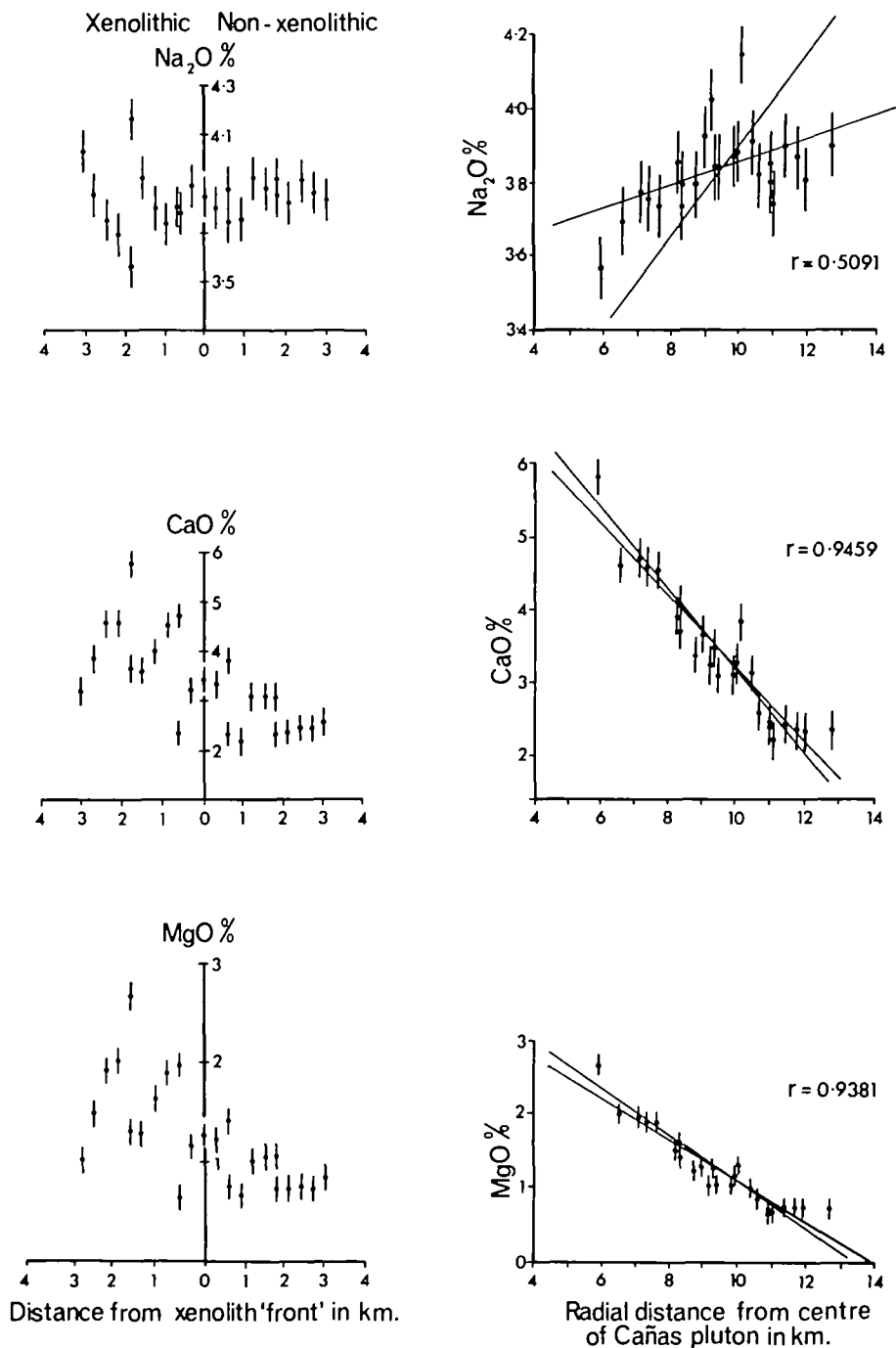


FIG. 8. Graphs showing the percentage of sodium, calcium, and magnesium oxides as a function of the distance from the xenolith 'front', and as a function of the radial distance from the centre of the Cañas pluton. In the graphs on the left-hand side of the figure, values from within the xenolith belt are plotted to the left of the central axis.

GEOLOGICAL PROCESS MODEL

A series of composite sections and their interpretation

The horizontal variation data obtained from the radially plotted graphs in Figs. 7 and 8 may now be combined with the vertical variation data obtained from the block diagrams in Figs. 3 and 4 to produce a series of composite radial cross-sections through the Puscao pluton, one for each oxide (Fig. 9).

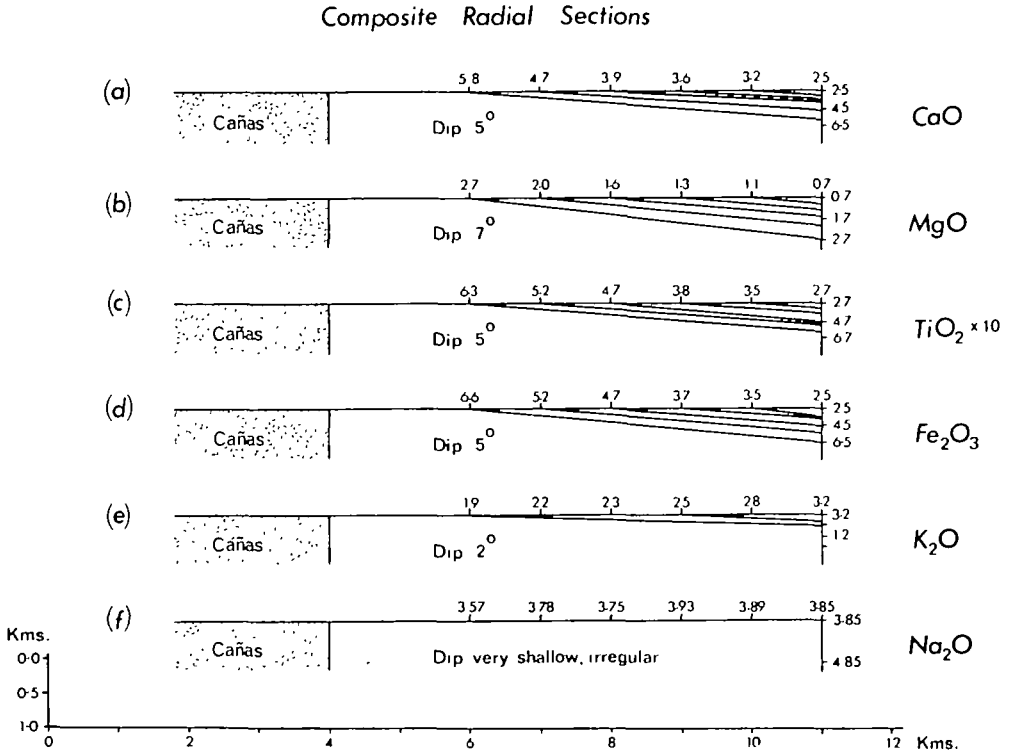


FIG. 9. Composite radial sections showing the relationship between the oxide distributions within the Puscao pluton and the position of the Cañas pluton.

Much of the scatter of plots on the graphs in Figs. 7 and 8 may be due to the absence of any allowance for the vertical component of variation. Nevertheless, actual plots were read off the graphs to construct the sections, rather than use values derived from the best fitting straight line which could be dismissed as purely theoretical. The use of the raw data is reflected in the variability of the dip within the various cross sections.

Despite these restrictions the picture presented by the composite radial sections is a remarkably consistent one, with a layered sequence dipping away from the Cañas pluton at a shallow angle, perhaps 5°.

Chemical variations which occur during a calc-alkaline differentiation sequence have been portrayed in the form of a number of variation diagrams by Gribble (1969). In Fig. 10 his curves for the six elements which have been studied in this

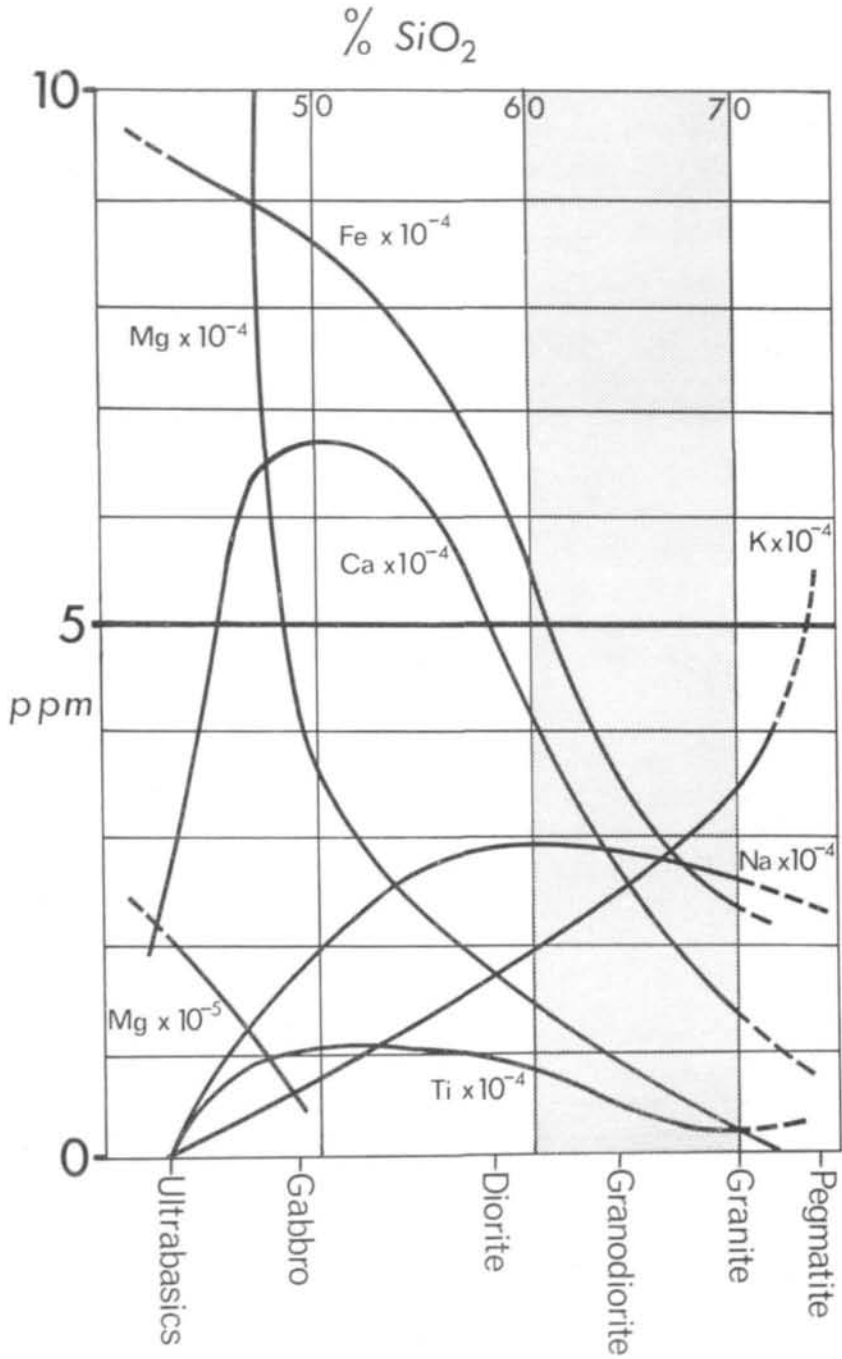


FIG. 10. Variation of the elements within a calc-alkaline differentiation sequence (after Gribble, 1969).

investigation are presented on a single variation diagram, and the range of rock types present within the sampled part of the Puscao pluton (based on silica determinations of selected specimens by X.R.F.) are shown shaded.

Within the shaded portion of Fig. 10 the amounts of the oxides of calcium, magnesium, titanium, and total iron increase towards the more basic members of the sequence. The oxide of potassium shows an increase in the opposite sense, being present in higher concentrations in the more acidic members, and the oxide of sodium shows little variation within the studied range.

The above data is so compatible with the variation observed in the Puscao pluton that it may be coupled with the composite radial cross-section results to produce a picture of a rather simple gravity differentiated pile. This finding is completely in accord with the field observations of large-scale layering within the Puscao pluton, reported by Cobbing & Pitcher (*op. cit.*), and noted in the introduction to this paper.

It seems likely that the radial dip of the differentiated pile away from the Cañas pluton is due to the doming of this layered sequence by the emplacement of the later Cañas pluton.

Although the vertical variation is readily appreciated in the field on a very large scale, it is virtually impossible to recognize on the scale of the composite sections. Fortunately the doming of the layered sequence is picked out by the attitude of the trains of xenoliths within the area studied. These xenoliths fell from a zone of instability in the roof on to the stratified crystal mush at intervals throughout its accumulation, in a similar manner to that described by Chapman (1969) for the Cadillac Mountain pluton in south-eastern Maine, U.S.A. Plate 1B is a view of the south-eastern wall of a dry quebrada in the Puscao pluton to the north-west of the Cañas pluton, and the dip of the xenolith trains away from the Cañas pluton (lying behind the ridge in the right of the photograph) can be clearly seen in the valley wall.

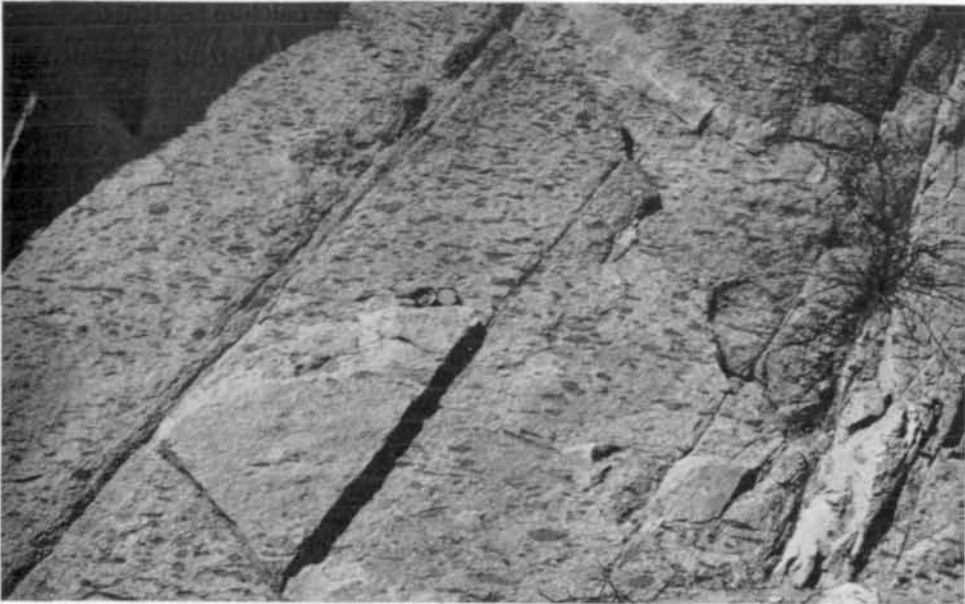
On the outcrop scale, the alignment of individual xenoliths parallel to the overall orientation of the xenolith trains is undoubtedly a primary feature, though it may have been accentuated by the limited deformation of the hot xenoliths due to the weight of the overlying crystal mush (Plate 1A).

This model of xenoliths continually 'cascading' down from a zone of structural weakness, such as pronounced jointing, in the roof also accounts for the rather well defined vertical, sub-planar margins of the xenolith belt.

PETROGRAPHY

Plagioclase

Plagioclase crystals occur mainly as individual subhedral crystals (1.0 to 2.0 mm long), having an elongation ratio of 2:1. When these crystals are in contact with one another the resulting interstitial spaces are filled with either quartz or alkali feldspar.



A



B

Plate 1

A. The general field appearance of xenoliths within the basified facies of the Puscao unit. Horizontal distance across the photograph is 3.5 m.

B. View of the xenolith trains within the Puscao pluton showing their relationship to the Cañas pluton (lying behind the ridge in the right of the photograph). Distance to the sky-line is approximately 200 m.

Most of the crystals are progressively zoned with the calcium content decreasing fairly uniformly from the centre (An_{41}) to the edge (An_{37}) with occasional weak oscillations.

In some cases, albite twinning is absent from the crystal and here the zoning appears to be more intricate than in the twinned varieties. This may be partly due to the cut effect, with the untwinned feldspar being later rim material, and this observation is borne out by its low relief when compared with the twinned examples.

The late rim material has modified many of the euhedral crystals of plagioclase, but the absence of twinning in the more sodic rim material enables one to see quite clearly the original euhedral outline of the core.

Alkali feldspar

The alkali feldspar is quite extensively altered to sericite but it is still possible to identify it as a perthite.

Most of the alkali feldspar in the thin sections occupies an interstitial position between euhedral crystals of plagioclase, biotite, and hornblende.

The relationship of the alkali feldspar to the quartz, which also appears late in the crystallization sequence, is often indeterminate, though on occasions the alkali feldspar exhibits well defined faces against the quartz.

Quartz

Quartz occurs both as small interstitial patches and also as larger areas enclosing euhedral plagioclase, biotite, and hornblende.

The relationship described in the preceding section suggests that the quartz is in fact later than some of the alkali feldspar, though much of the quartz and alkali feldspar appear to have crystallized simultaneously.

Biotite

The usual pleochroic scheme of the biotite is $X =$ yellowish brown, $Y = Z =$ very dark brown.

The biotite occurs as isolated crystals having well developed (001) faces against quartz and alkali feldspar and also as small clusters associated with hornblende, iron ore, and sphene.

Many of the isolated crystals of biotite often have small euhedral crystals of randomly oriented twinned plagioclase enclosed within them. Hornblende is often included as well formed prisms within the clusters of biotite flakes.

There is extensive alteration of the biotite to chlorite with the production of minor amounts of epidote.

Hornblende

The most common pleochroic scheme of the hornblende is $X =$ yellow-green, $Y =$ olive-green, and $Z =$ blue-green.

The hornblende is often associated with biotite and iron ore, with some elongate (3:1) euhedral prisms of hornblende occasionally being found in isolation. The well-formed prisms of hornblende are often partially enclosed within the biotite crystals, suggesting that the crystallization of hornblende slightly preceded that of biotite.

Accessory minerals

Epidote is present in small amounts, and appears to be associated with the breakdown of biotite into chlorite rather than being due to the saussuritization of the plagioclase feldspar.

Skeletal sphene and opaque ores are also present in the vicinity of mafic minerals. The absence of these minerals from the plagioclase crystals and their inclusion within the mafic minerals suggests that they crystallized after the zoned plagioclases but before the mafic minerals.

Crystallization of the pluton

In the light of the wet chemical results, four sample powders were chosen so as to be representative of the range of samples used in this study. Complete major oxide analyses were performed on these selected powders, enabling their normative compositions to be calculated. In Fig. 11, these compositions are shown plotted on the diagram of predicted phase relations in the system An–Ab–Or–SiO₂–H₂O due to Carmichael (1963).

A probable crystallization path for the Puscao magma has been drawn through the plots and the resulting sequence of crystallization is consistent with that deduced from the petrography.

Unfortunately since this investigation was confined to only part of the Puscao pluton, and Puscao lithologies are present elsewhere that fall outside the range studied, the author is unable to predict an original magma composition for the pluton as a whole.

Throughout the thin sections there is little sign of the preferred orientation of minerals which one might expect in the light of the supposed large scale layering. In other layered bodies such as the Stillwater complex, Montana (*e.g.* Hess, 1960 and Jackson, 1961) or Skaergaard, Greenland (Wager & Deer, 1939) a planar fabric (and at times a linear fabric) can be detected due to the preferred orientation of the plagioclase feldspar laths.

When one considers the factors influencing the rotational stability of plagioclase laths as they settle on to the Puscao crystal mush, the high viscosity of the acid magma, the low value of the elongation ratio of the plagioclase feldspars (2:1), and the low density contrast between the plagioclase feldspar and the magma, would probably not result in highly unstable conditions. The plagioclase crystals would therefore be relatively unaffected by the gravitational orientation, and would tend to have a much more random orientation.

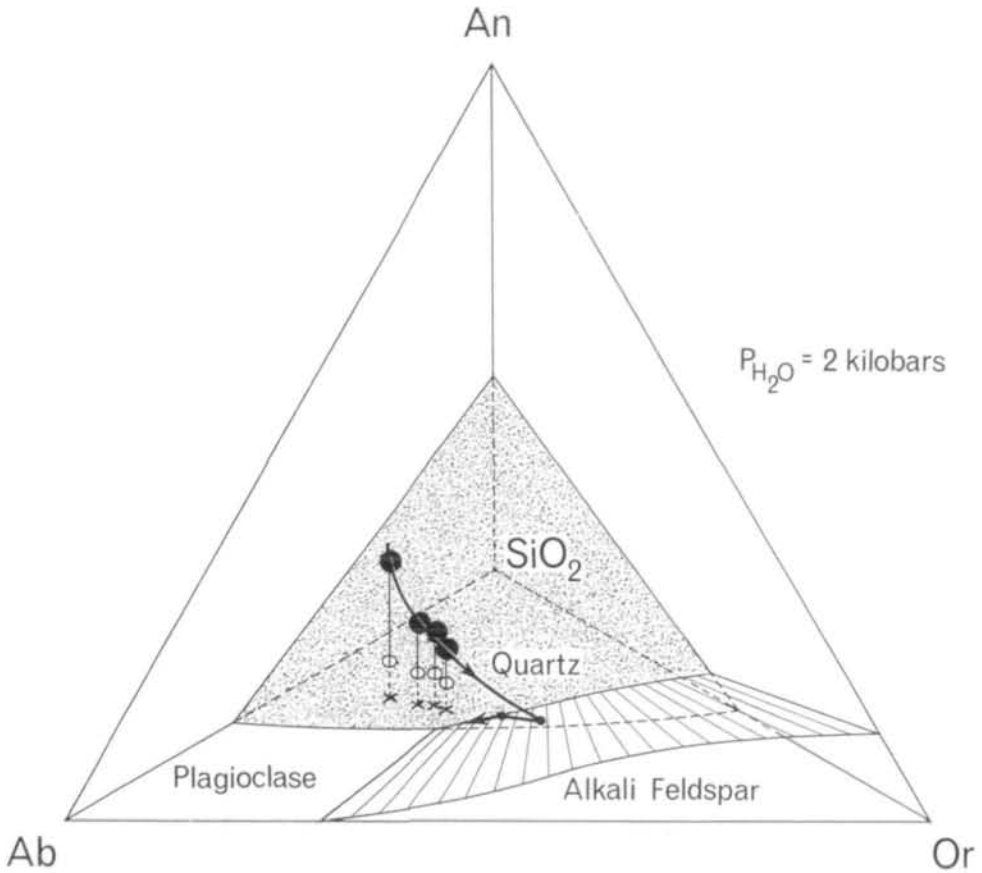


FIG. 11. Probable crystallization path of the Puscao magma based on plots of compositions chosen so as to be representative of the range of samples used in this study. The predicted phase relations in the system An-Ab-Or-SiO₂-H₂O are those of Carmichael (1963).

This effect seems to have prevailed even in some of the much less viscous magmas of the layered granites of Southern Greenland described by Harry & Emeleus (1960) and Emeleus (1963).

The crystallization processes within the Puscao magma chamber apparently failed to produce the fluctuations in the availability of mafic minerals which gave rise to the rhythmic layering of the granites of Southern Greenland and enabled Harry & Emeleus (*op. cit.*) and Emeleus (*op. cit.*) to recognize gravity stratification and trough banding. If the formation of rhythmic layering is due to the influence of 'some variable factor' on the magmatic volatiles, as concluded by Harry & Emeleus (*op. cit.*), the fact that the Puscao magma appears to have been much less charged with volatiles than the fluorite-bearing granites of Southern Greenland would certainly explain the absence of rhythmic layering in the Puscao case.

CONCLUSIONS

Although the single field season, the man-hours available for analysis, and the original concept of large scale xenolithic contamination imposed limitations on the sampling scheme, the author has been able to bring to light certain features of the Puscao pluton which may be applicable elsewhere.

The process of contamination, which may be important locally, is subordinate to that of differentiation in controlling the overall chemistry of the pluton. Whether this result is also true for granites emplaced at a lower level in the crust remains to be seen.

The usefulness of trend-surface work in granitic terrain needs to be carefully re-examined in view of the marked vertical component of variation which has been recognized in the field as well as in the regression surface analysis. This need for reappraisal was spotlighted by Whitten (1961) and Peikert (1962), but later workers, *e.g.* Morton *et al.* (1969), have continued to use the trend-surface approach.

Observation of a gentle updoming associated with cauldron subsidence emplacement within stratified piles of either sediments or lavas is fairly well documented, *e.g.* Rast *et al.* (1968). The author believes, however, that this is the first time that such an updoming associated with cauldron subsidence emplacement has been recognized within a wholly plutonic country-rock.

The close compatibility of the results of the regression surface analysis techniques with the field observations, and the simplicity of the process model which may be postulated as a result of their use, are clear indications of the usefulness of this powerful method in the investigation of granitic bodies.

ACKNOWLEDGEMENTS

The author would like to thank Professor W. S. Pitcher and Dr. M. P. Atherton for the time spent in useful discussions and in reading and criticizing the manuscript. Thanks are also extended to M. S. Brotherton for his guidance during the modification of the computer program and during the initial stages of the chemical analysis. The Computer Laboratory staff at the University of Liverpool have on innumerable occasions offered advice on the best solutions for the many small computational problems, as and when they arose.

In conclusion, the author acknowledges the financial support which N.E.R.C. has kindly given to the Peru Project in general and to the author in particular in the form of a Studentship.

REFERENCES

- ATHERTON, M. P., & BRENCHLEY, P. J., 1972. A preliminary study of the structure, stratigraphy, and metamorphism of some contact rocks of the Western Andes, near the Quebrada Venado Muerto, Peru. *Geol. J.* **8**, 161–78.
- BROTHERTON, M. S., & RAISWELL, R., 1971. A comparison of automatic and manual wet chemical analysis of rocks. *Chem. Geol.* **7**, 285–93.
- BAIRD, A. K., MCINTYRE, D. B., & WELDAY, E. E., 1967. Geochemical and structural studies in the batholithic rocks of Southern California. Part II. Sampling of the Rattlesnake Mountain Pluton for chemical composition, variability, and trend analysis. *Bull. geol. Soc. Am.* **78**, 191–221.
- BUDDINGTON, A. F., 1959. Granite emplacement with special reference to North America. *Ibid.* **70**, 671–747.
- CARMICHAEL, I. S. E., 1963. The crystallization of feldspar in volcanic acid liquids (with discussion). *Q. Jl geol. Soc. Lond.* **119**, 95–131.
- CHAPMAN, C. A., 1969. Oriented inclusions in granite—further evidence for floored magma chambers. *Am. J. Sci.* **267**, 988–98.
- CHAYES, F., 1970. On deciding whether trend surfaces of progressively higher order are meaningful. *Bull. geol. Soc. Am.* **81**, 1273–78.
- COBBING, E. J., & PITCHER, W. S., 1972. The Coastal Batholith of central Peru. *J. geol. Soc. Lond.* **128**, 421–60.
- EMELEUS, C. H., 1963. Structural and petrographic observations on layered granites from Southern Greenland. *Miner. Soc. Am. Spec. Pap.* **1**, 22–9.
- GRIBBLE, C. D., 1969. Distribution of elements in igneous rocks of the normal calc alkaline sequence. *Scot. J. Geol.* **5**, 322–7.
- GREEN, J., & POLDERVAART, A., 1958. Petrochemical fields and trends. *Geochim. Cosmochim. Acta*, **13**, 87–122.
- HARRY, W. T., & EMELEUS, C. H., 1960. Mineral layering in some granite intrusions of SW. Greenland. *Rept. 21st Int. geol. Congr. (Norden)*. **14**, 172–81.
- HESS, H. H., 1960. Stillwater igneous complex, Montana: a quantitative mineralogical study. *Mem. geol. Soc. Am.* **80**.
- JACKSON, E. D., 1961. Primary textures and mineral associations in the Ultramafic Zone of the Stillwater complex, Montana. *Prof. Pap. U.S. geol. Surv.* **358**, 1–106.
- KNOX, G. J., 1974. The structure and emplacement of the Rio Fortaleza centred acid complex, Ancash, Peru. *Jl. geol. Soc. Lond.* **130**, 295–308.
- MERCY, E. L. P., 1956. The accuracy and precision of rapid methods of silicate analysis. *Geochim. Cosmochim. Acta*, **9**, 161–73.
- MORTON, D. M., BAIRD, A. K., & BAIRD, K. W., 1969. The Lakeview Mountains pluton, Southern California Batholith. Part II. Chemical composition and variation. *Bull. geol. Soc. Am.* **80**, 1553–64.
- PEIKERT, E. W., 1962. Three-dimensional specific-gravity variation in the Glen Alpine Stock, Sierra Nevada, California. *Ibid.* **73**, 1437–42.
- RAST, N., DIGGENS, J. N., & RAST, D. E., 1968. Triassic rocks of the Isle of Mull; their sedimentation, facies, structure, and relationship to the Great Glen Fault and the Mull caldera. (A demonstration.) *Proc. geol. Soc. Lond.* **1645**, 299–305.
- SAMPSON, R. J., & DAVIS, J. C., 1967. Three-dimensional response surface program in Fortran II for the I.B.M. 1620 computer. *Kansas geol. Surv. Computer Contrib.* **10**.
- WAGER, L. R., & DEER, W. A., 1939. Geological investigations in East Greenland, Pt. 3. The petrology of the Skaergaard Intrusion, Kangerlugssuaq, East Greenland. *Meddr. Grønland* **105**, 1–352.
- WHITTEN, E. H. T., 1961. Quantitative distribution of major and trace components in rock masses. *Trans. Am. Inst. Min. Engrs.* **220**, 239–46.